# Transformation of $Au_{144}(SCH_2CH_2Ph)_{60}$ to $Au_{133}(SPh\text{-}tBu)_{52}$ Nanomolecules: Theoretical and Experimental Study

Praneeth Reddy Nimmala,[†] Shevanuja Theivendran,[†] Giovanni Barcaro,[‡] Luca Sementa,[‡] Chanaka Kumara,[†] Vijay Reddy Jupally,[†,⊥] Edoardo Apra,[§] Mauro Stener,[∥] Alessandro Fortunelli,*[,‡] and Amala Dass*[,†]

[†]Department of Chemistry and Biochemistry, University of Mississippi, Oxford, Mississippi 38677, United States

[‡]CNR-ICCOM & IPCF, Consiglio Nazionale delle Ricerche, Pisa I-56124, Italy

[§]Pacific Northwest National Laboratory, William R. Wiley Environmental Molecular Sciences Laboratory, Richland, Washington 99352, United States

[∥]Dipartimento di Scienze Chimiche e Farmaceutiche, Università di Trieste, Trieste I-34127, Italy

**ABSTRACT:** Ultrastable gold nanomolecule $Au_{144}(SCH_2CH_2Ph)_{60}$ upon etching with excess *tert*-butylbenzenethiol undergoes a core-size conversion and compositional change to form an entirely new core of $Au_{133}(SPh\text{-}tBu)_{52}$. This conversion was studied using high-resolution electrospray mass spectrometry which shows that the core size conversion is initiated after 22 ligand exchanges, suggesting a relatively high stability of the $Au_{144}(SCH_2CH_2Ph)_{38}(SPh\text{-}tBu)_{22}$ intermediate. The $Au_{144} \rightarrow Au_{133}$ core size conversion is surprisingly different from the $Au_{144} \rightarrow Au_{99}$ core conversion reported in the case of thiophenol, −SPh. Theoretical analysis and ab initio molecular dynamics simulations show that rigid *p*-*t*Bu groups play a crucial role by reducing the cluster structural freedom, and protecting the cluster from adsorption of exogenous and reactive species, thus rationalizing the kinetic factors that stabilize the $Au_{133}$ core size. This 144-atom to 133-atom nanomolecule's compositional change is reflected in optical spectroscopy and electrochemistry.

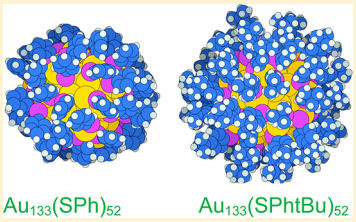


Au-thiolate nanomolecules on reacting with excess thiol at elevated temperature[1] can lead to either (a) a complete ligand exchange or (b) core-size conversion to form an entirely new core-size.[2] For example, reacting $Au_{144}(SCH_2CH_2Ph)_{60}$ with (a) hexanethiol leads to formation of $Au_{144}(SC_6H_{13})_{60}$, that is, ligand exchange (b) whereas the same reaction when performed in an aromatic thiol, thiophenol yields $Au_{99}(SPh)_{42}$, that is, core size conversion.[3] This thermochemical treatment at elevated temperature is well established through the reports by Whetten's group and is referred to as "etching".[1] This procedure has then been widely followed and has been used by Murray, Tsukuda, Whetten and other groups[4−6] to synthesize and characterize stable nanomolecules, including $Au_{25}(SR)_{18}$, $Au_{38}(SR)_{24}$, and $Au_{144}(SR)_{60}$.[7−9] This procedure has also been recently called by a new name "size-focusing".[10] Although size-focusing can occur during the etching process, this is not always the case, as this can lead to either (a) complete ligand exchange or (b) core size conversion. The core-size conversion resulting from the etching process can also depend on the *nature of the ligand*. Etching a mixture containing ~12 kDa species, $Au_{67}$ and $Au_{103-105}$ in the presence of phenylethanethol results in the formation of $Au_{38/40}(SR)_{24}$. However, etching the same mixture with thiophenol leads to the formation of $Au_{36}(SPh)_{24}$.[11,12] However, the principles governing these exchange and conversion are not yet fully clarified.

Etching reaction has a crucial role in the synthesis of $Au_{38}$. $Au_{38}(SR)_{24}$ has been synthesized using etching reactions first reported as the 8 kDa species by Whetten in 1999.[1] Tsukuda group identified this 8 kDa species as $Au_{38}(SR)_{24}$ in 2008 using high resolution ESI mass spectrometry.[8] Quinn group also reported the synthesis of $Au_{38}(SC_6H_{13})_{24}$.[13] Using the same etching procedures, Jin's group also reported the "size focusing synthesis" of $Au_{38}(SR)_{24}$.[14] It has been shown that $Au_{38}(SR)_{24}$ is formed exclusively from larger clusters as a result of core-size conversion.[11]

Here, we report an experimental and theoretical analysis of the core size conversion of ultrastable $Au_{144}(SCH_2CH_2Ph)_{60}$ upon reaction with excess *tert*-butyl benzene thiol, leading to the formation of $Au_{133}(SPh\text{-}tBu)_{52}$. As a striking result, we find that changing the ligand shell in regions remote from the gold core (i.e., adding a *tert*-butyl substituent in para position to the thiolate phenyl ring) leads to a different product, with a completely different size and composition: $Au_{133}(SPh\text{-}tBu)_{52}$ vs $Au_{99}(SPh)_{42}$. This is shown to be due to *kinetic factors* whose importance in the synthesis of gold−thiolate nanomolecules is so unequivocally demonstrated by both experiment and theory. First-principles molecular dynamics (MD) simulations addi-

**Accepted:** May 18, 2015

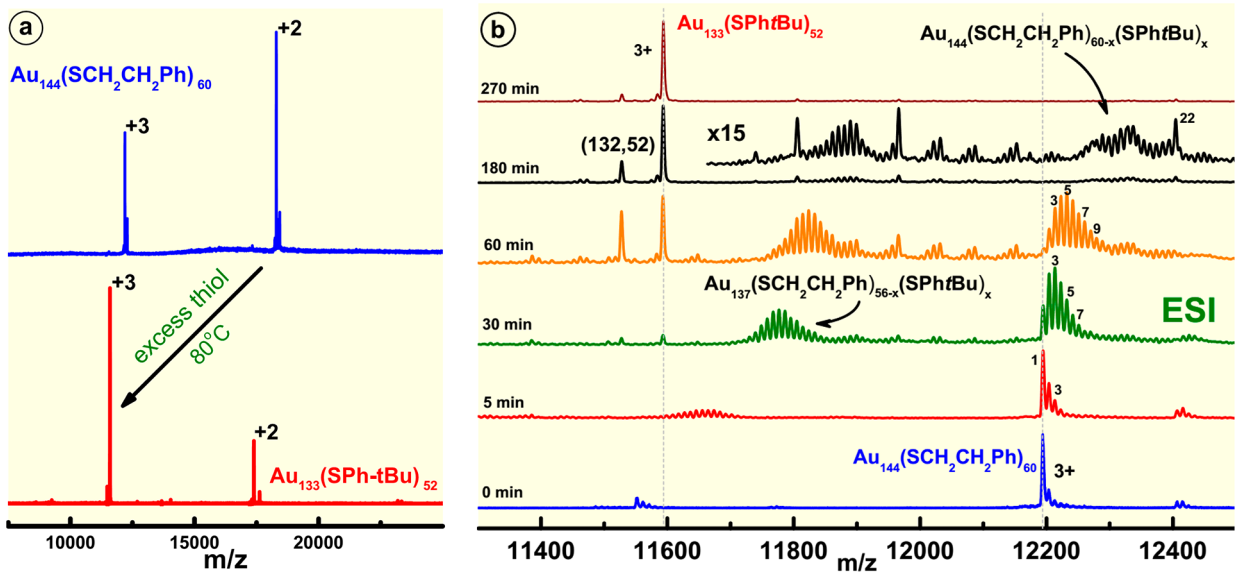


**Figure 1.** Core size conversion of $Au_{144}(SCH_2CH_2Ph)_{60}$ to $Au_{133}(SPh\text{-}tBu)_{52}$: (a) Electrospray ionization mass spectra of the monodisperse $Au_{144}(SCH_2CH_2Ph)_{60}$ starting material (top blue spectrum) transforming to $Au_{133}(SPh\text{-}tBu)_{52}$ (bottom red spectrum) upon treatment with HSPh-*t*Bu at 80 °C. (b) $Au_{144}$ to $Au_{133}$ core size conversion studied by ESI mass spectrometry. $Au_{144}(SCH_2CH_2Ph)_{60}$ undergoes up to 22 ligand exchanges. The intermediates correspond to $Au_{144}(SCH_2CH_2Ph)_{60-x}(SPh\text{-}tBu)_x$ where $x$ = 1 to 22. Note the higher stability corresponding to $x$ = 22, based on higher signal intensity. After 22 exchanges, there appears to be a core size conversion to $Au_{133}(SPh\text{-}tBu)_{52}$. In contrast, thiophenol (HSPh) reacts with $Au_{144}(SCH_2CH_2Ph)_{60}$ to form $Au_{99}(SPh)_{42}$, with a maximum of 13 exchanges in $Au_{144}(SCH_2CH_2Ph)_{60-x}(SPh)_x$.

tionally provide insight into the mechanisms of structural dynamics in a large Au nanomolecule.

The X-ray crystal structure[15,16] of $Au_{133}(SPh\text{-}tBu)_{52}$ has been reported recently.[17,18] In Figure 1a, the blue spectra shows the electrospray ionization (ESI) mass spectra (MS) of the starting material, $Au_{144}(SCH_2CH_2Ph)_{60}$ with a molecular weight of 36 597 Da. The multiply charged +2 and +3 ions at 18 291 and 12 194 $m/z$ respectively. The final product is shown in the red spectrum, which contains two peaks at slightly lower mass than $Au_{144}$ species. These two peaks at 11 594 and 17 391 $m/z$ correspond to the +3 and +2 ions of $Au_{133}(SPh\text{-}tBu)_{52}$, respectively. The theoretical values for the +3 and +2 ions are 11 597 and 17 396, respectively. Because the starting material, $Au_{144}(SR)_{60}$ is clean without any other core-size nanoparticles, it is clear that the 144-atom core size has transformed into the 133-atom nanomolecule due to the effect of the −SPh-*t*Bu groups. The final product is clean without any other core sizes and the yield of the product is >90% (Au atom basis).

Figure 1b shows the ESI-MS study of the ligand exchange induced core size conversion from $Au_{144}$ to $Au_{133}$.

The ligand exchange reaction process has been monitored using ESI-MS in order to analyze the formation of $Au_{133}(SPh\text{-}tBu)_{52}$ from $Au_{144}(SCH_2CH_2Ph)_{60}$. The molecular weight of phenylethanethiol and *tert*-butylbenzenethiol are 137.2 and 165.2 Da, respectively, which gives a mass difference of 28 Da. From the ESI-MS spectra shown in Figure 1b, the peak at 12194 $m/z$ corresponds to +3 charge state of the starting material. In 30 min sample, an envelope of peaks was observed corresponding to the $Au_{144}(SCH_2CH_2Ph)_{60-x}(SPh\text{-}tBu)_x$, where $x_{max}$ is ∼7 *tert*-butylbenzenethiolates. The exchanges continue to occur with $Au_{144}(SCH_2CH_2Ph)_{60}$ until 180 min. Thereafter, a peak seems to appear at 11 594 Da, which corresponds to +3 of $Au_{133}(SPh\text{-}tBu)_{52}$. Simultaneously, the set of peaks corresponding to the ligand exchange have reached $Au_{144}(SCH_2CH_2Ph)_{60-x}$ $(SPh\text{-}tBu)_x$, where $x$ is ∼22 *tert*-butylbenzenethiolates. The exchange with 22 ligands seems to be higher in stability based on the relatively greater intensity of the peak in ESI-MS compared to other peaks and could be due to exchange at specific sites.[19] The 270 min sample shows the peak that has completely core converted to $Au_{133}(SPh\text{-}tBu)_{52}$. Note that there is an additional peak at a slightly lower mass corresponding to $Au_{132}(SPh\text{-}tBu)_{52}$. Moreover, another envelope of peaks corresponding to ligand exchange with $Au_{137}(SCH_2CH_2Ph)_{60}$ were also observed in 30 and 60 min samples. This could be due to the residual $Au_{137}(SCH_2CH_2Ph)_{56}$ present in the starting material.[20] However, it is important to make a note that the exchange of ligands with $Au_{137}$ is much faster than that of $Au_{144}$. Also, the sharp peaks at 11 968 and 11 805 correspond to $Au_{137}(SPh\text{-}tBu)_{44}(SCH_2CH_2Ph)_{12}$ and $Au_{137}(SPh\text{-}tBu)_{27}(SCH_2CH_2Ph)_{29}$, respectively. Higher intensity of these peaks indicates the relatively greater stability of these intermediates. Three other peaks were also observed as the intermediates of size conversion. They are the peaks at 12 033, 12 086, and 12 153 $m/z$ units, corresponding to +3 of $Au_{137}(SPh\text{-}tBu)_{51}(SCH_2CH_2Ph)_5$, $Au_{138}(SPh\text{-}tBu)_{50}(SCH_2CH_2Ph)_6$, and $Au_{139}(SPh\text{-}tBu)_{50}(SCH_2CH_2Ph)_6$, respectively.

The optical and electrochemical properties of the starting material, $Au_{144}(SCH_2CH_2Ph)_{60}$ and the end product, $Au_{133}(SPh\text{-}tBu)_{52}$ are directly compared.[21,22] The blue curve in Figure 2a is for the starting material $Au_{144}(SCH_2CH_2Ph)_{60}$. It has minor features at 510 and 700 nm as reported previously. The end product $Au_{133}(SPh\text{-}tBu)_{52}$, shown in red curve, exhibits no distinctly observable peaks but some minor peaks at 510 and 430 nm. The peak at 510 nm is not to be confused with the SPR peak at 530 nm because there are no larger clusters in the starting material (the absence of SPR in the starting material indicates that no higher clusters >$Au_{144}$ were present) and etching reactions are typically top-down where larger clusters breakdown to smaller more stable clusters, whereas the opposite is not observed. The electrochemical behavior of $Au_{133}(SPh\text{-}tBu)_{52}$ is also uniquely different than

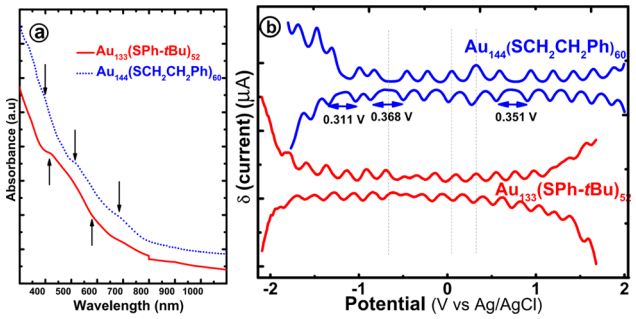


**Figure 2.** (a) UV−vis absorption spectrum of $Au_{133}(SPh\text{-}tBu)_{52}$ nanomolecules in toluene (red curve) in comparison with the starting material $Au_{144}(SCH_2CH_2Ph)_{60}$ (blue curve). (b) Electrochemistry. DPV of $Au_{144}(SCH_2CH_2Ph)_{60}$ used as a starting product (in blue), compared with that of $Au_{133}(SCH_2Ph\text{-}tBu)_{52}$, the end product (in red). The DPV were acquired in anhydrous 1,2-dichloroethane solution with 0.5 mM bis(triphenyl phosphoranylidene) ammonium tetrakis (pentafluorophenyl) borate [$BTPPATBF_{20}$] as supporting electrolyte under nitrogen atmosphere.

$Au_{144}(SCH_2CH_2Ph)_{60}$ measured under identical conditions as shown in Figure 2b. Seventeen redox waves were observed in the voltammogram of $Au_{133}(SPh\text{-}tBu)_{52}$. However, the redox behavior was significantly different than the $Au_{144}(SR)_{60}$, which exhibits three distinct ~350 mV spacing centered at −1.2, −0.8, +0.8 V. Though $Au_{133}$ is smaller than $Au_{144}$ no eletrochemical gap was observed. This could be attributed to the difference in the structure and ligands of these two nanomolecules, which could result in the difference in the energy levels. A previous report on the electrochemical analysis of $Au_{36}(SPh)_{24}$ has also showed that ligand and structure have strong influence on the electrochemical[23] and optical properties of gold nanomolecules. Also, the electrochemical properties of $Au_{133}$ are different compared to $Au_{130}(SR)_{50}$, which showed an electrochemical gap of 450 mV.[2] Indeed, although $Au_{133}(SPh\text{-}tBu)_{52}$ is close in composition to the $Au_{130}(C_{12}H_{25})_{50}$ nanomolecule reported by Negishi et al. (produced in etching a crude mixture of higher clusters), it is possible that the geometry of these two clusters is entirely different from each other. This was the case with $Au_{38}$ and $Au_{36}$ where the former had an bi-icosahedral core, whereas the latter had an FCC core. Indirect structural information can be deduced from the above optical and electrochemical characterization.

$Au_{144}(SR)_{60}$ is regarded as a highly stable cluster from its ability to withstand harsh thermochemical treatment for about 24 h at 80 °C in the same thiol, which is protected with (SR = phenylethanethiol, hexanethiol, or dodecanethiol). But when treated with an aromatic ligand *tert*-butylbenzenethiol, its core is converted to $Au_{133}$ in just 2 h at 80 °C (depending on the ratio of nanocluster to incoming ligand). This has been so far interpreted as due to the aromatic ligands conjugating effect, which enhances the rate of reaction. Both thiophenol (-HSPh) and *tert*-butylthiophenol (HSPh-*t*Bu) lead to the formation of $Au_{36}(SPh\text{-}X)_{24}$, where $x$ = H or *t*Bu. The larger size $Au_{144}(SCH_2CH_2Ph)_{60}$ was core converted to $Au_{99}(SPh)_{42}$ upon etching with thiophenol. From the results on $Au_{36}$ and the conversion of $Au_{144}(SCH_2CH_2Ph)_{60}$ to $Au_{99}(SPh)_{42}$, it would seem reasonable and logical to expect that a similar conversion occurs with para-*tert*-butylthiophenol. The results reported above show that surprisingly, etching $Au_{144}(SCH_2CH_2Ph)_{60}$ with HSPh-*t*Bu yields $Au_{133}(SPh\text{-}tBu)_{52}$. Theoretical analysis can provide understanding of the extent that the bulky para-*t*Bu groups can influence the structural conversion of $Au_{144}$.

The equilibrium structural properties of the $Au_{133}(SPh\text{-}tBu)_{52}$ nanocrystal molecule were addressed in ref 17. Here, we extend structural analysis to dynamical features. The main question on the $Au_{144} \rightarrow Au_{133}$ core size conversion is why $Au_{99}(SPh)_{42}$ is not formed by simply adding a *t*Bu substituent in para position in the thiol.

The role of the *p*-*t*Bu groups in stabilizing the $Au_{133}(SPh\text{-}tBu)_{52}$ cluster is 2-fold.

First, the *p*-*t*Bu groups reduce the cluster structural freedom by significantly reducing the dynamic dispersion of surface bonds in $Au_{133}(SPh\text{-}tBu)_{52}$ with respect to $Au_{133}(SPh)_{52}$. To prove this quantitatively, AIMD runs at 900 K on the two nanomolecules (this high value of temperature is chosen to acquire a significant statistics in a limited AIMD run time) are analyzed, and the quantities

$$[CC(S-C)\_ij(t) - \langle CC(S-C)\_ij \rangle]$$

are extracted, where $t$ is the time step of the AIMD, CC(S−C)_ij is the bond length between a sulfur atom and the phenyl carbon atom bound to it, and <CC(S−C)_ij> is the corresponding time average over the entire AIMD run. Such quantities are plotted in Figure 3, where one can see that

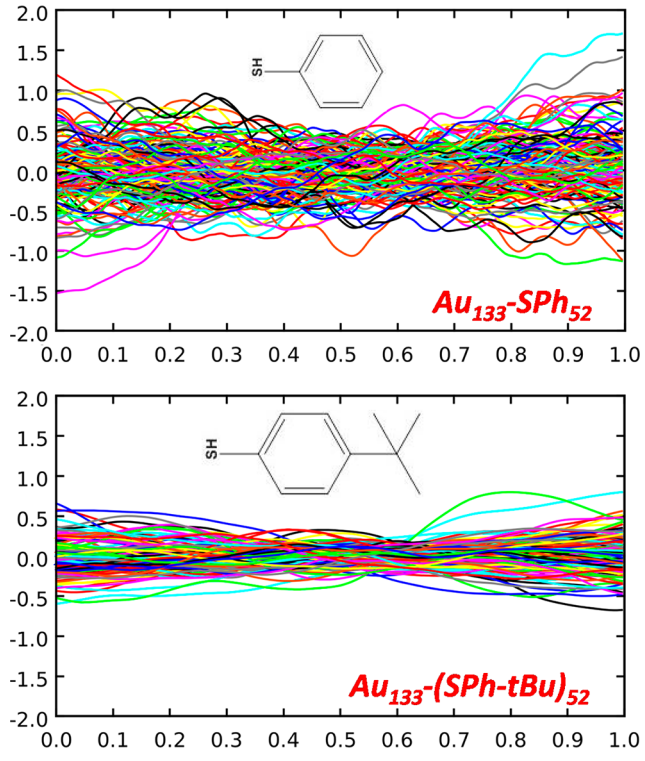


**Figure 3.** Plots of [CC(S−C)_ij - <CC(S−C)_ij>] quantities extracted from AIMD runs on $Au_{133}(SPh)_{52}$ (top) and $Au_{133}(SPh\text{-}tBu)_{52}$ (bottom) nanomolecules. Ordinates in angstroms. Time in picoseconds.

dynamic fluctuations are much more pronounced when *p*-*t*Bu substituents are absent (an even more pronounced difference is found when plotting the dispersion of orientational degrees of freedom at the surface, not shown). The greater structural dispersion of S−C bonds extracted from AIMD runs of $Au_{133}(SPh)_{52}$ with respect to $Au_{133}(SPh\text{-}tBu)_{52}$ demonstrates that the *p*-*t*Bu substituents decrease the cluster fluxional

character (also due to the increase in the mass of the thiolate ligands by addition of the *tert*-butyl groups) and confirms the stabilizing role of such bulky and massive groups, for example, in increasing energy barriers for detachment/addition of thiolate ligands (kinetic stabilization). To further illustrate this point, in Figure 4 typical facile movements (rotation/slight-

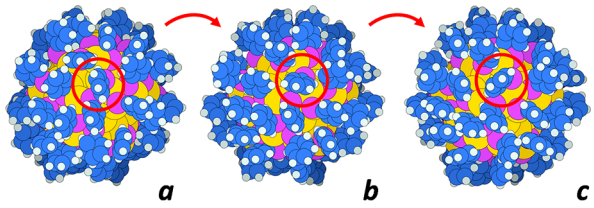


**Figure 4.** Snapshots extracted from a MD run on $Au_{133}(SPh)_{52}$ illustrating typical rotation/bending movements (a → b, b → c) occurring in such systems (see text for more details).

bending) occurring during the MD run on $Au_{133}(SPh)_{52}$ are shown. Such movements are much less facile and frequent in $Au_{133}(SPh\text{-}tBu)_{52}$. Finally, it should be noted that in our simulations the Au atoms are frozen in the experimentally determined geometry (see the Synthesis of $Au_{133}(SPh\text{-}tBu)_{52}$ via Ligand Exchange section). We make this choice to focus on the reasons why etching stops at the $Au_{133}$ core size, rather than fully simulating the etching process. It can be added that the crystallographically determined Au core geometry in $Au_{133}(SPh\text{-}tBu)_{52}$ has strong structural analogies with the structural model for $Au_{144}(SCH_2CH_2Ph)_{60}$ as discussed in ref 17, which further supports our choice of freezing the Au core.

Second, the *p*-*t*Bu groups play an important role in providing a protective outer layer, which prevents exogenous species (such as solvent molecules) from adsorbing on the surface of the Au cluster, reducing the likelihood of reactive processes and facilitating X-ray analysis. This is pictorially illustrated in Figure 5 by a visual comparison of the structures of the two

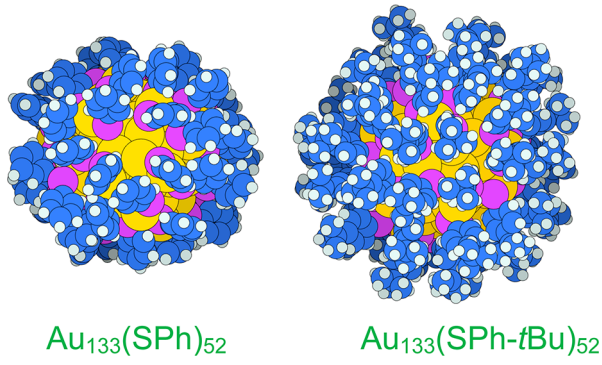


**Figure 5.** Visual comparison of $Au_{133}(SPh)_{52}$ (left) and $Au_{133}(SPh\text{-}p\text{-}tBu)_{52}$ (right) illustrating the empty space in the former nanomolecule filled by the *p*-*t*Bu substituents in the latter.

nanomolecules, in which the larger "holes" formed on the nanomolecule surface in the absence of *p*-*t*Bu substituents can be immediately visualized.

Summarizing, at this Au core size and radius of the coating shell a reduction in the sulfur surface density necessarily creates empty space among the organic residues, and therefore a geometric instability with phenyl rings oscillating among different positions and the formation of "holes" in the coating layer. The *p*-*t*Bu groups help alleviating this issue thus stabilizing the structure.

Moreover, at the opposite of the common understanding, the role of phenyl electronic conjugation on the stability of $Au_{133}(SPh\text{-}tBu)_{52}$ is minor. This is proved by a comparison of the electronic total energies of $Au_{133}(SPh\text{-}tBu)_{52}$ and a species in which electronic conjugating effects are absent such as $Au_{133}(SCH_3)_{52}$. The reaction energy of the ligand replacement process:

$$Au_{133}(SPh\text{-}tBu)_{52} + 52HSCH_3 \rightarrow Au_{133}(SCH_3)_{52} + 52HSPh\text{-}tBu \quad (1)$$

has been calculated. Because this energy is quite sensitive to the geometric structure of the reactants, we do not use any experimental input and the geometries of all compounds in eq 1 are fully optimized at the DFT/PBE level. Interestingly, this reaction energy turns out to be negative: −6.6 eV. It should be underlined that we do not intend to model via eq 1 a real ligand replacement process, but rather to provide an assessment of electronic conjugation effects. The fact that the reaction energy in eq 1 is negative simply shows that conjugation effects on stability must be minor. However, only electronic contributions are included in eq 1, which neglects entropic and environmental terms that play an important thermodynamic role[24] and may well change the thermodynamic driving force to ligand displacement. Indeed, if we add dispersion terms (a component of solvation effects) as a Grimme-type semiempirical correction to the total energy, the reaction energy of eq 1 changes sign: from −6.6 to +9.7 eV.

Finally, it is interesting is to estimate the residual steric repulsion in the ligand shell of $Au_{133}(SPh\text{-}tBu)_{52}$. As noted in ref 17, replacement of nonbulky ligands as in $Au_{144}(SCH_2CH_2Ph)_{60}$ with bulkier phenyl groups creates a steric repulsion in proximity of the Au cluster, which is alleviated by decreasing the thiolate surface density. Indeed, the average surface area per sulfur atom increases from 18.8 Å$^2$ to 19.2 Å$^2$ in passing from $Au_{144}S_{60}$ to $Au_{133}S_{52}$. To estimate the residual steric repulsion, a recently proposed energy decomposition analysis protocol[24] is used, via a comparison between the energy of 52 RS thiolate ligands in their optimized geometry in the gas-phase with the energy of the same 52 ligands but *frozen* in the geometry extracted from the optimized structure of the $Au_{133}(SPh\text{-}tBu)_{52}$ cluster, that is, a $[(SPh\text{-}tBu)_{52}]$ "crown" of ligands. Moreover, to eliminate the interaction among S atoms in the crown and obtain a cleaner estimate of steric hindrance, we take the difference of this quantity between the $[(SPh\text{-}tBu)_{52}]$ ligands from $Au_{133}(SPh\text{-}tBu)_{52}$ and a $[(SCH_3)_{52}]$ crown of ligands obtained by putting S and C atoms in the same positions as the $[(SPh\text{-}tBu)_{52}]$ and only relaxing the hydrogen atoms. Assuming that the steric repulsion in the $[(SCH_3)_{52}]$ crown is negligible, this difference provides an estimate of steric repulsion in $[(SPh\text{-}tBu)_{52}]$: the value so obtained is 1.6 eV, which is rather small given the size of the system. In short, in $Au_{133}(SPh\text{-}tBu)_{52}$ the radius of the Au core and the ligand surface density is such that steric repulsion is minimized. The residual repulsion is not due to the *t*Bu groups but rather to the phenyl groups, as is proven by the fact that the repulsion energy is practically the same in a $Au_{133}(SPh)_{52}$ compound obtained by replacing the *p*-*t*Bu substituents with hydrogens.

In conclusion, $Au_{133}(SPh\text{-}tBu)_{52}$ is the first report on the core conversion of the stable $Au_{144}(SCH_2CH_2Ph)_{60}$ nanocluster.

The steric effect of the *p*-*t*Bu groups provides rigidity to the cluster thereby improving the crystallinity and purity of the materials which is crucial for the crystal formation and total structure determination. Interesting future directions include chiral separation,[25] alloy formation,[26] and other theoretical analysis.[27,28]

## EXPERIMENTAL SECTION

*Synthesis of $Au_{133}(SPh\text{-}tBu)_{52}$ via Ligand Exchange.* The synthesis and isolation of $Au_{133}(SPh\text{-}tBu)_{52}$ was performed in two steps. The first step involves the synthesis of $Au_{144}(SCH_2CH_2Ph)_{60}$ using two-phase Brust–Schiffrin method.[35] A crude polydisperse mixture of $Au_{144}$ was synthesized in a two phase reaction and further etched and purified using size exclusion chromatography. In a second step, the monodisperse product (>90%) $Au_{144}(SCH_2CH_2Ph)_{60}$ was subjected to ligand exchange with *tert*-butylbenzenethiol.

Step 1: $HAuCl_4{\cdot}3H_2O$ (0.3 g) dissolved in distilled water (30 mL) and TOABr (0.42 g, Au:TOABr = 1:1) dissolved separately in toluene (30 mL) were mixed together in a 250 mL round-bottom flask under 500 rpm of stirring. The orange-red solution was stirred for about 30 min. When all the Au salt was transferred to the organic layer, it was separated from the aqueous layer and phenylethanethiol (Au:thiol = 1:4) was added. The solution was stirred for another 1 h, until the orange-red solution turned turbid. At this point, $NaBH_4$ (0.29g, Au:NaBH4 = 1:10) was added rapidly into the reaction mixture. The solution turned black indicating the formation of nanomolecules. The stirring was continued for 3 h and the resultant product was dried using rotary evaporation in order to remove excess solvent. The crude product was washed with methanol 3–4 times to remove excess thiol and other reaction byproducts. The product was then etched in phenylethanethiol for ∼12 h (200 mg of crude sample in 2 mL of phenylethanethiol in a 10 mL round-bottom flask at 80 °C and 500 rpm) and $Au_{144}(SCH_2CH_2Ph)_{60}$ were isolated by size exclusion chromatography.

Step 2: The second stage involves ligand exchange of pure $Au_{144}(SCH_2CH_2Ph)_{60}$ with 4-*tert*-butylbenzenethiol for 4 h at room temperature to obtain the desired final product $Au_{133}(SPh\text{-}tBu)_{52}$.

*Mass Spectrometry.* MALDI mass spectra were acquired using Bruker AutoFlex 1 and using DCTB matrix.[29] ESI-MS analysis was performed using Waters Synapt HDMS instrument and sample mixed with 50:50 toluene:$CH_3CN$ or 50:50 THF:$CH_3CN$ solvent system. $Au_{25}(SCH_2CH_2Ph)_{18}$ and $Au_{144}(SCH_2CH_2Ph)_{60}$ were used for calibration checks.

*First-Principles Simulations.* As in ref 17, local geometry relaxations and Ab Initio Molecular Dynamics (AIMD) runs were performed using the CP2K[30] whose DFT algorithms are based on a hybrid Gaussian/Plane-Wave scheme (GPW[31] The Perdew–Burke–Ernzerhof (PBE) exchange-correlation (xc-) functional[32] was employed. Pseudopotentials derived by Goedecker, Teter, and Hutter were chosen to describe the core electrons of all[33] and DZVP basis sets[34] to represent the DFT Kohn–Sham orbitals. The cutoff for the auxiliary plane wave representation of the density was 300 Ry. AIMD runs used a time step of 1.0 fs and the temperature was controlled by Nosé–Hoover chain thermostats.[36] The $Au_{133}$ core was kept frozen during the AIMD simulations, assuming that the positions of these heavy atoms were correctly determined by X-ray measurements.

## AUTHOR INFORMATION


### Corresponding Authors

*E-mail: amal@olemiss.edu.

*E-mail: alessandro.fortunelli@cnr.it.

### Present Address

[⊥](V.R.J.) Intel Corporation, 2501 NW 229th Avenue, Hillsboro, Oregon 97124, United States.


### Notes

The authors declare no competing financial interest.

## ACKNOWLEDGMENTS


The experimental portion of the research was funded through NSF-CHE-1255519. A portion of the computational research was performed using PNNL Institutional Computing at Pacific Northwest National Laboratory.


## REFERENCES


(1) Schaaff, T. G.; Whetten, R. L. Controlled Etching of Au: SR Cluster Compounds. *J. Phys. Chem. B* **1999**, *103*, 9394–9396.

(2) Jupally, V. R.; Dass, A. Synthesis of $Au_{130}(SR)_{50}$ and $Au_{130-x}Ag_x(SR)_{50}$ Nanomolecules Through Core Size Conversion of Larger Metal Clusters. *Phys. Chem. Chem. Phys.* **2014**, *16*, 10473–10479.

(3) Nimmala, P. R.; Dass, A. $Au_{99}(SPh)_{42}$ Nanomolecules: Aromatic Thiolate Ligand Induced Conversion of $Au_{144}(SCH_2CH_2Ph)_{60}$. *J. Am. Chem. Soc.* **2014**, *136*, 17016–17023.

(4) Negishi, Y. A Critical Size for Emergence of Nonbulk Electronic and Geometric Structures in Dodecanethiolate-Protected Au Clusters. *J. Am. Chem. Soc.* **2015**, *137*, 1206–1212.

(5) Tvedte, L. M.; Ackerson, C. J. Size-Focusing Synthesis of Gold Nanoclusters with *p*-Mercaptobenzoic Acid. *J. Phys. Chem. A* **2014**, *118*, 8124–8128.

(6) Udayabhaskararao, T.; Pradeep, T. New Protocols for the Synthesis of Stable Ag and Au Nanocluster Molecules. *J. Phys. Chem. Lett.* **2013**, *4*, 1553–1564.

(7) Parker, J. F.; Fields-Zinna, C. A.; Murray, R. W. The Story of a Monodisperse Gold Nanoparticle: $Au_{25}L_{18}$. *Acc. Chem. Res.* **2010**, *43*, 1289–1296.

(8) Chaki, N. K.; Negishi, Y.; Tsunoyama, H.; Shichibu, Y.; Tsukuda, T. Ubiquitous 8 and 29 kDa gold: Alkanethiolate Cluster Compounds: Mass-Spectrometric Determination of Molecular Formulas and Structural Implications. *J. Am. Chem. Soc.* **2008**, *130*, 8608–8610.

(9) Schaaff, T. G.; Shafigullin, M. N.; Khoury, J. T.; Vezmar, I.; Whetten, R. L. Properties of a Ubiquitous 29 kDa Au: SR Cluster Compound. *J. Phys. Chem. B* **2001**, *105*, 8785–8796.

(10) Jin, R.; Qian, H.; Wu, Z.; Zhu, Y.; Zhu, M.; Mohanty, A.; Garg, N. Size Focusing: A Methodology for Synthesizing Atomically Precise Gold Nanoclusters. *J. Phys. Chem. Lett.* **2010**, *1*, 2903–2910.

(11) Nimmala, P. R.; Jupally, V. R.; Dass, A. Core Size Conversion: Route for Exclusive Synthesis of $Au_{38}$ or $Au_{40}$ Nanomolecules. *Langmuir* **2014**, *30*, 2490–2497.

(12) Nimmala, P. R.; Dass, A. $Au_{36}(SPh)_{23}$ Nanomolecules. *J. Am. Chem. Soc.* **2011**, *133*, 9175–9177.

(13) Toikkanen, O.; Ruiz, V.; Ronholm, G.; Kalkkinen, N.; Liljeroth, P.; Quinn, B. M. Synthesis and Stability of Monolayer-Protected $Au_{38}$ Clusters. *J. Am. Chem. Soc.* **2008**, *130*, 11049–11055.

(14) Qian, H.; Zhu, Y.; Jin, R. Size-Focusing Synthesis, Optical and Electrochemical Properties of Monodisperse $Au_{38}(SC_2H_4Ph)_{24}$ Nanoclusters. *ACS Nano* **2009**, *3*, 3795–3803.

(15) Jadzinsky, P. D.; Calero, G.; Ackerson, C. J.; Bushnell, D. A.; Kornberg, R. D. Structure of a Thiol Monolayer-Protected Gold Nanoparticle at 1.1 Angstrom Resolution. *Science* **2007**, *318*, 430–433.

(16) Qian, H.; Zhu, M.; Wu, Z.; Jin, R. Quantum Sized Gold Nanoclusters with Atomic Precision. *Acc. Chem. Res.* **2012**, *45*, 1470–79.

(17) Dass, A.; Theivendran, S.; Nimmalla, P.; Kumara, C.; Jupally, V.; Fortunelli, A.; Sementa, L.; Barcaro, G.; Zuo, X.; Noll, B. C. $Au_{133}(SR)_{52}$ Nanomolecules: X-ray Crystallography, Optical, Electrochemical, and Theoretical Analysis. *J. Am. Chem. Soc.* **2015**, *137*, 4610−4613.
(18) Zeng, C.; Chen, Y.; Kirschbaum, K.; Appavoo, K.; Sfeir, M. Y.; Jin, R. Structural Patterns at All Scales in a Nonmetallic Chiral $Au_{133}(SR)_{52}$ Nanoparticle. *Sci. Adv.* **2015**, *1*, 31500045.
(19) Heinecke, C. L.; Ni, T. W.; Malola, S.; Mäkinen, V.; Wong, O. A.; Häkkinen, H.; Ackerson, C. J. Structural and Theoretical Basis for Ligand Exchange on Thiolate Monolayer Protected Gold Nanoclusters. *J. Am. Chem. Soc.* **2012**, *134*, 13316−13322.
(20) Jupally, V. R.; Dharmaratne, A. C.; Crasto, D.; Huckaba, A. J.; Kumara, C.; Nimmala, P. R.; Kothalawala, N.; Delcamp, J. H.; Dass, A. $Au_{137}(SR)_{56}$ Nanomolecules: Composition, Optical Spectroscopy, Electrochemistry and Electrocatalytic Reduction of $CO_2$. *Chem. Commun.* **2014**, *50*, 9895−9898.
(21) Alvarez, M. M.; Khoury, J. T.; Schaaff, T. G.; Shafigullin, M. N.; Vezmar, I.; Whetten, R. L. Optical Absorption Spectra of Nanocrystal Gold Molecules. *J. Phys. Chem. B* **1997**, *101*, 3706−3712.
(22) Murray, R. W. Nanoelectrochemistry: Metal Nanoparticles, Nanoelectrodes, and Nanopores. *Chem. Rev.* **2008**, *108*, 2688−2720.
(23) Nimmala, P. R.; Knoppe, S.; Jupally, V. R.; Delcamp, J. H.; Aikens, C. M.; Dass, A. $Au_{36}(SPh)_{24}$ Nanomolecules: X-ray Crystal Structure, Optical Spectroscopy, Electrochemistry, and Theoretical Analysis. *J. Phys. Chem. B* **2014**, *118*, 14157−14167.
(24) Crasto, D.; Barcaro, G.; Stener, M.; Sementa, L.; Fortunelli, A.; Dass, A. $Au_{24}(SAdm)_{16}$ Nanomolecules: X-ray Crystal Structure, Theoretical Analysis, Adaptability of Adamantane Ligands to Form $Au_{23}(SAdm)_{16}$ and $Au_{25}(SAdm)_{16}$, and Its Relation to $Au_{25}(SR)_{18}$. *J. Am. Chem. Soc.* **2014**, *136*, 14933−14940.
(25) Dolamic, I.; Knoppe, S.; Dass, A.; Bürgi, T. First Enantioseparation and Circular Dichroism Spectra of $Au_{38}$ Clusters Protected by Achiral Ligands. *Nat. Commun.* **2012**, *3*, 798.
(26) Negishi, Y.; Kurashige, W.; Niihori, Y.; Nobusada, K. Toward the Creation of Stable, Functionalized Metal Clusters. *Phys. Chem. Chem. Phys.* **2013**, *15*, 18736−18751.
(27) Aikens, C. M. Electronic Structure of Ligand-Passivated Gold and Silver Nanoclusters. *J. Phys. Chem. Lett.* **2010**, *2*, 99−104.
(28) Hakkinen, H. The Gold−Sulfur Interface at the Nanoscale. *Nat. Chem.* **2012**, *4*, 443−455.
(29) Dass, A.; Stevenson, A.; Dubay, G. R.; Tracy, J. B.; Murray, R. W. Nanoparticle MALDI-TOF Mass Spectrometry without Fragmentation: $Au_{25}(SCH_2CH_2Ph)_{18}$ and Mixed Monolayer $Au_{25}(SCH_2CH_2Ph)_{18-x}(L)_x$. *J. Am. Chem. Soc.* **2008**, *130*, 5940−5946.
(30) Hutter, J.; Iannuzzi, M.; Schiffmann, F.; VandeVondele, J. Cp2k: Atomistic Simulations of Condensed Matter Systems. *Wiley Interdiscip. Rev.: Comput. Mol. Sci.* **2014**, *4*, 15−25.
(31) Lippert, G.; Hutter, J.; Parrinello, M. The Gaussian and Augmented-Plane-Wave Density Functional Method for Ab Initio Molecular Dynamics Simulations. *Theor. Chem. Acc.* **1999**, *103*, 124−140.
(32) Perdew, J. P.; Burke, K.; Ernzerhof, M. Generalized Gradient Approximation Made Simple. *Phys. Rev. Lett.* **1996**, *77*, 3865−3868.
(33) Goedecker, S.; Teter, M.; Hutter, J. Separable Dual-Space Gaussian Pseudopotentials. *Phys. Rev. B* **1996**, *54*, 1703−1710.
(34) VandeVondele, J.; Hutter, J. Gaussian Basis Sets for Accurate Calculations on Molecular Systems in Gas and Condensed Phases. *J. Chem. Phys.* **2007**, *127*, 114105.
(35) Brust, M.; Walker, M.; Bethell, D.; Schiffrin, D. J.; Whyman, R. Synthesis of Thiol-Derivatised Gold Nanoparticles in a Two-Phase Liquid-Liquid System. *J. Chem. Soc., Chem. Commun.* **1994**, 801−802.
(36) Martyna, G. J.; Klein, M. L.; Tuckerman, M. Nosé−Hoover chains: The Canonical Ensemble via Continuous Dynamics. *J. Chem. Phys.* **1992**, *97*, 2635−2643.